

PUBLISHED VERSION

Badalyan, Alexander; Carageorgos, Themis; Bedrikovetski, Pavel; You, Zhenjiang; Zeinijahromi, Abbas; Aji, Keyiseer

[Critical analysis of uncertainties during particle filtration](#)

Review of Scientific Instruments, 2012; 83(9):095106

© 2012 American Institute of Physics.

Copyright 2012 American Institute of Physics. This article may be downloaded for personal use only. Any other use requires prior permission of the author and the American Institute of Physics.

The following article appeared in Review of Scientific Instruments, 2012; 83(9):095106 and may be found at http://rsi.aip.org/resource/1/rsinak/v83/i9/p095106_s1.

PERMISSIONS

http://www.aip.org/pubservs/web_posting_guidelines.html

“On the authors' and employers' webpages:

- There are no format restrictions; files prepared and/or formatted by AIP or its vendors (e.g., the PDF, PostScript, or HTML article files published in the online journals and proceedings) may be used for this purpose. If a fee is charged for any use, AIP permission must be obtained.
- An [appropriate copyright notice](#) must be included along with the full citation for the published paper and a [Web link to AIP's official online version of the abstract](#).”

12th March 2013

<http://hdl.handle.net/2440/74959>

Critical analysis of uncertainties during particle filtration

Alexander Badalyan, Themis Carageorgos, Pavel Bedrikovetsky, Zhenjiang You, Abbas Zeinijahromi et al.

Citation: *Rev. Sci. Instrum.* **83**, 095106 (2012); doi: 10.1063/1.4749844

View online: <http://dx.doi.org/10.1063/1.4749844>

View Table of Contents: <http://rsi.aip.org/resource/1/RSINAK/v83/i9>

Published by the [American Institute of Physics](#).

Related Articles

Elementary steps of the catalytic NO_x reduction with NH₃: Cluster studies on reactant adsorption at vanadium oxide substrate

J. Chem. Phys. **138**, 094704 (2013)

Titanium catalyzed silicon nanowires and nanoplatelets

AIP Advances **3**, 032112 (2013)

Photodissociation of methyl iodide adsorbed on low-temperature amorphous ice surfaces

J. Chem. Phys. **138**, 084703 (2013)

Communication: Structure, formation, and equilibration of ensembles of Ag-S complexes on an Ag surface

J. Chem. Phys. **138**, 071101 (2013)

Thiolate adsorption on Au(hkl) and equilibrium shape of large thiolate-covered gold nanoparticles

J. Chem. Phys. **138**, 064702 (2013)

Additional information on Rev. Sci. Instrum.

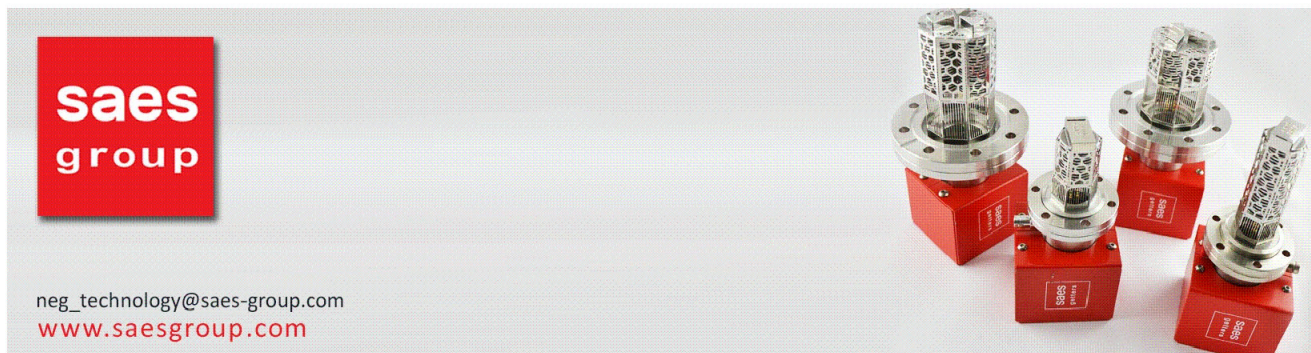
Journal Homepage: <http://rsi.aip.org>

Journal Information: http://rsi.aip.org/about/about_the_journal

Top downloads: http://rsi.aip.org/features/most_downloaded

Information for Authors: <http://rsi.aip.org/authors>

ADVERTISEMENT



saes
group

neg_technology@saes-group.com
www.saesgroup.com

Critical analysis of uncertainties during particle filtration

Alexander Badalyan,^{a)} Themis Carageorgos, Pavel Bedrikovetsky, Zhenjiang You, Abbas Zeinijahromi, and Keyiseer Aji

Australian School of Petroleum, University of Adelaide, Adelaide, South Australia 5005, Australia

(Received 30 April 2012; accepted 19 August 2012; published online 11 September 2012)

Using the law of propagation of uncertainties we show how equipment- and measurement-related uncertainties contribute to the overall combined standard uncertainties (CSU) in filter permeability and in modelling the results for polystyrene latex microspheres filtration through a borosilicate glass filter at various injection velocities. Standard uncertainties in dynamic viscosity and volumetric flowrate of microspheres suspension have the greatest influence on the overall CSU in filter permeability which excellently agrees with results obtained from Monte Carlo simulations. Two model parameters “maximum critical retention concentration” and “minimum injection velocity” and their uncertainties were calculated by fitting two quadratic mathematical models to the experimental data using a weighted least squares approximation. Uncertainty in the internal cake porosity has the highest impact on modelling uncertainties in critical retention concentration. The model with the internal cake porosity reproduces experimental “critical retention concentration vs velocity”-data better than the second model which contains the total electrostatic force whose value and uncertainty have not been reliably calculated due to the lack of experimental dielectric data. © 2012 American Institute of Physics. [<http://dx.doi.org/10.1063/1.4749844>]

I. INTRODUCTION

Experimental^{1,2} and theoretical³ approaches for description of deep bed filtration successfully coexist and complement each other leading to improvement in process design in petroleum and geothermal water processes, in environmental processes and other areas dealing with particles migration. Microparticles attachment due to electrostatic attraction to the surface of a porous medium can be studied using colloidal suspension flow through an engineered porous medium. The chemistry and hydrodynamics of the colloidal suspension, surface chemistry of colloids and porous media, and particle and pore sizes are important parameters in the particle attachment process. Attachment of particles onto a porous medium is accompanied by reduction in its permeability due to the deposit of colloidal particles that decrease the cross-sectional area available for suspension flow. The colloids deposition process can be monitored by measuring the permeability decline. This deposition can be reliably determined if experimental uncertainty in the permeability of a porous medium is known. Despite its importance, the uncertainties in experimental permeability data during coreflood tests are not routinely implemented in laboratory investigations and not much attention has been given in the literature.

Nevertheless, Kwon *et al.*⁴⁻⁶ graphically determined permeability of shale specimens to NaCl solutions with standard deviation of 1%–3% excluding any errors in the evaluation of pressure drop across the shale specimen, dynamic viscosity, and compressibility of NaCl solutions. Applying the law of propagation of uncertainties and Monte Carlo simulation to Darcy equation, Dong⁷ identified uncertainties in viscosity and pressure as the major sources of uncertainty in permeability. Mazumder and Wolf⁸ applied an error analysis to

Darcy equation and experimental data of sub- and supercritical CO₂ flow through coal samples. Uncertainty in pressure gradient along the coal specimen was the major contributor to the overall uncertainty in permeability of around 20%.

Good reproducibility of permeability measurements is important for comparison of experimental data from intra- and inter-laboratory tests.⁹ Brighenti and Macini indicated that “a standardization of permeability measurement procedure is necessary, in order to ensure reliable comparisons amongst different sets of data.”¹⁰ Such standardization is difficult to achieve due to: unavailability of “certified permeability standards from recognised standard institutions,”¹¹ and the limited information about experimental uncertainties for permeability and particle concentration data.

Theoretical models for different particle capture mechanisms have been developed and represent the respective experimental data with various degrees of agreement.¹²⁻¹⁵ However, according to Al-Abduwani *et al.*,¹⁶ validation of such models via different experimental methods is limited. Additionally, unavailability of uncertainty analyses for models describing suspension transport in porous media and limited information about uncertainties for the respective experimental data makes validation of such models difficult.

In the present work, a detailed and systematic analysis of experimental and modelling uncertainties associated with permeability measurements during colloidal particle attachment to an engineered porous medium is done. Particle attachment during colloidal suspension injection at different velocities was monitored via real-time measurements of the porous medium permeability and post-experimental colloids mass balance. The law of propagation of uncertainties was applied for calculation of uncertainties in parameters of Darcy equation. Parameters having the greatest effect on uncertainties in permeability and modelling results were identified, and recommendations for reducing modelling uncertainties

^{a)} Author to whom correspondence should be addressed. Electronic mail: alexander.badalyan@adelaide.edu.au.

TABLE I. Chemical composition of a borosilicate glass filter.

Compound	SiO ₂	B ₂ O ₃	Na ₂ O ₃	Al ₂ O ₃	CaO	Cl	MgO	Fe ₂ O ₃
%, w/w	80.60	12.60	4.20	2.20	0.10	0.10	0.05	0.04

were presented. Recommendations from NIST¹⁷ and EURACHEM¹⁸ uncertainty guidelines were used in this paper.

II. MATERIALS

A. Borosilicate glass filter

A borosilicate sintered glass filter (ROBU[®], Glasfilter-Geraete GmbH, Hattert, Germany), with pore sizes varying within 10–16 μm (from now on called filter) was used as porous medium. Chemical composition of this filter according to the manufacturer is given in Table I. The filter porosity was determined as 43% by the Archimedes method.

B. Colloidal latex particles

Polystyrene latex microspheres crafted by surface carboxyl groups (Polysciences, Inc., Warrington, PA) were used for the preparation of colloidal suspension. According to the manufacturer, these microspheres have a mean diameter of $d_{c,mean} = 1.019 \pm 0.032 \mu\text{m}$ which translates to the mean jamming ratio of $j = \frac{d_{c,mean}}{d_{pore,mean}} = 0.08$.

The colloidal suspension was prepared by adding the microspheres to a 0.1 M NaCl aqueous solution at pH 3. In these conditions there is almost no self-agglomeration, bridging or size exclusion capture.^{19,20}

III. EXPERIMENTAL SECTION

A. Experimental setup

A schematic diagram of the setup for filter permeability measurements is shown in Fig. 1. The filter 1 is held inside a rubber sleeve 2 located in a high-pressure core holder 3. An overburden pressure is established by pumping MilliQ water through a manual valve 4 (Swagelok[®]), and measured by a Bourdon tube pressure gauge 5 (Swagelok). The colloidal suspension was pumped through the filter by a high-performance liquid chromatography (HPLC) pump 6 (Scientific Systems, Inc., Lab Alliance, PA) via a manual valve 7 (Swagelok). A back-pressure regulator 8 (Swagelok) maintains the pore pressure at the desired level.

The pore pressure is measured by a PA 33X gauge pressure transmitter 9 (KELLER AG fur Druckmesstechnik, Winterthur, Switzerland). Differential pressure across the filter is measured by four differential pressure transducers 10–13 (DPTs) (Validyne Engineering, CA) with different measuring ranges. Manual valves 14–17 connect a respective DPT to a flow-through system. Each DPT is connected to a respective readout/signal conditioner. Output signals from readouts/signal conditioners (0 to 10 Vdc) and PA 33X (0–5 Vdc) enter the analog input channels of the ADAM-4019+ analog-to-digital data acquisition module 18 (Advantech[®], Taipei, Taiwan), which via the ADAM-5060 RS-232/RS-485/RS-422

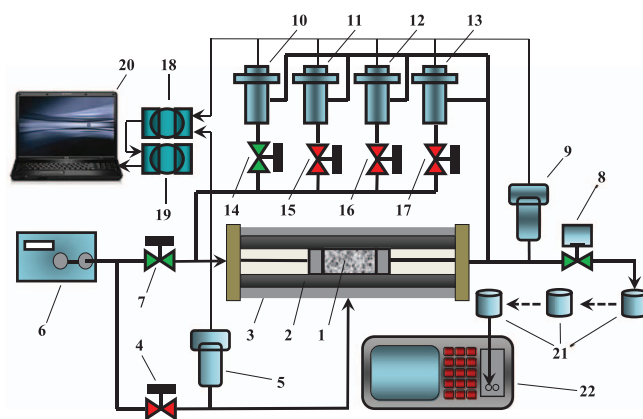


FIG. 1. Schematic of a real-time data acquisition and monitoring system for liquid permeability of porous media. (“Green” colour denotes open valves, “red” colour denotes closed valves.) (1) Filter; (2) rubber sleeve; (3) high-pressure core holder; (4, 7, 14–17) manual valves; (5) Bourdon tube pressure gauge; (6) HPLC pump; (8) back-pressure regulator; (9) PA 33X gauge pressure transmitter; (10–13) Validyne differential pressure transducers; (18) ADAM-4019+ data acquisition module; (19) ADAM-5060 RS-232/RS-485/RS-422 signal converter; (20) personal computer; (21) beakers; (22) PAMAS S4031 GO portable particle counter.

signal converter 19 (Advantech, Taipei, Taiwan) is incorporated into a real-time data acquisition and monitoring system based on stand-alone personal computer 20. Custom build data acquisition software based on Advantech ADAMView 4.25 application builder calculates and records differential pressures in real time. Dynamic data exchange server delivers all experimental data (temperature, pressure, differential pressure, and time) into Microsoft Excel incorporating all corresponding calculations and graphs.

Particle deposition in the filter was studied at following velocities: 1.32×10^{-3} , and $(7.92, 3.96, 2.64, \text{ and } 1.32) \times 10^{-4}$ m/s. Continuous monitoring of the filter permeability in real-time provided information about attachment of colloidal particles: stabilisation of monotonically reduced permeability within experimental uncertainty in filter permeability (3.09%) assumed the end of particle attachment process for the chosen flowrate. As an example, the decrease of filter permeability with particle deposition at velocity of 1.32×10^{-4} m/s is shown in Fig. 2 (vertical bars indicate the CSU in permeability).

The effluent stream was collected in plastic beakers 21 (Figure 1), and particle concentrations in the inlet and outlet streams were determined by PAMAS S4031 GO portable particle counter 22 (PAMAS GmbH, Salzuflen, Germany). The difference between these concentrations determines the volumetric concentration of the attached particles. Later, this concentration was converted to dimensionless (reduced by the volume of the filter) volumetric concentration or critical retention concentration. The following relationship was experimentally established (Fig. 3):

$$\sigma_{cr} = \sigma_{cr}(U), \quad (1)$$

where $\sigma_{cr}(U)$ is critical retention concentration of attached particles; and U is velocity, m/s. Particle deposition at 1.32×10^{-3} and 7.92×10^{-4} m/s resulted in negligibly low values of critical retained concentrations and their CSUs which are

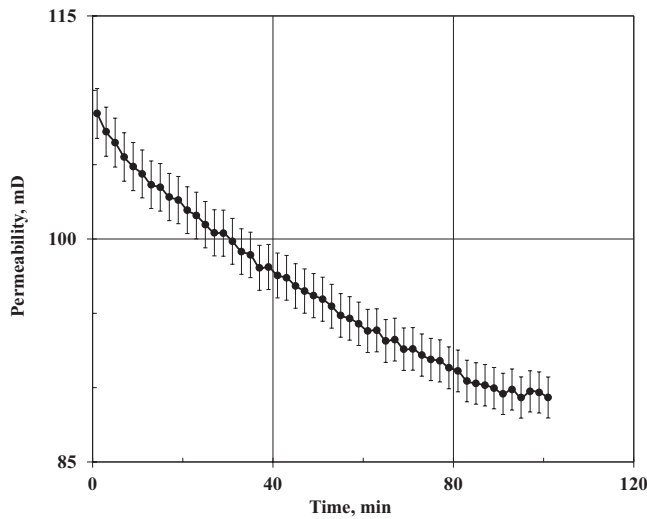


FIG. 2. Variation of glass filter permeability during colloid deposition at 1.32×10^{-4} m/s.

not included in all consecutive calculations and, therefore, not shown in Fig. 3.

B. Metrological characteristics of instrumentation

Manufacturer-supplied metrological characteristics of instruments used in the setup are the primary source of equipment-related uncertainties used for calculation of measurement-related uncertainties in parameters of Darcy equation, particle concentrations, and modelling results (see Table II).

Output signal from type-T thermocouple (not shown in Fig. 1) together with those from readouts/signal conditioners and PA 33 X are fed into ADAM-4019+. Taking into account the accuracy and 16-bit resolution of ADAM-4019+ and NIST^{17,21} recommendations, CSUs in temperature, dif-

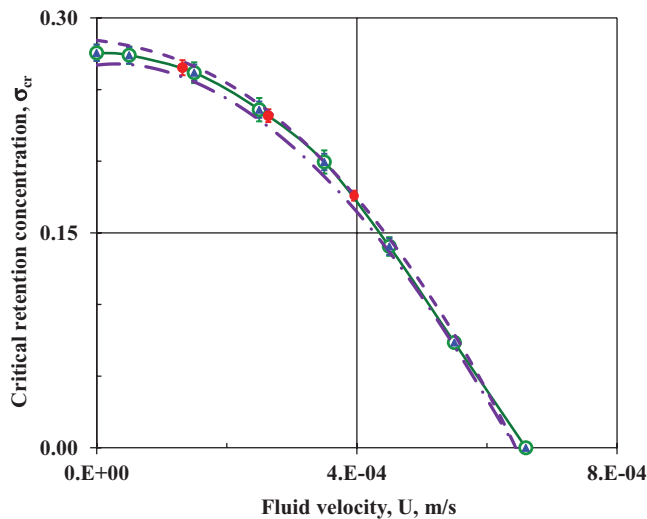


FIG. 3. Comparison of experimental data and modelled results for critical retention particle concentration. ● experimental data; ▲ quadratic function model fitting using OLSM; ○ quadratic function model fitting using WLSM; - - - lower uncertainty limit for Eq. (14); - - - upper uncertainty limit for Eq. (14).

TABLE II. Metrological characteristics of instrumentation.

Instrument	Measuring range	Accuracy
HPLC pump	0–100 ml/min	2.0% FS
Type-T thermocouple	N/A	1.0 K
ADAM 4019+	0–5; 10 Vdc	0.1%
Valydine DPT	0–(8.62×10^3 ; 8.62×10^4 ; 8.62×10^5 ; 8.62×10^6) Pa	0.25% FS
PA 33X	0.1–30 MPa	0.1 FS

Note: FS means full scale.

ferential pressure, and absolute pressure of suspension were calculated (see Table III).

The manufacturer calibrated PAMAS using NIST traceable particles without stating its accuracy which is necessary for the evaluation of uncertainties in inlet and outlet particle concentrations. We evaluated the PAMAS repeatability by measuring number of particles across various particle size distributions for the investigated particle size. Ten consecutive measurements of particle numbers resulted in a standard deviation of $u(N_{particle}^{PAMAS}) = 4402$ or 1.75% for a narrow particle diameter range from 0.904 to 1.126 μm . Since PAMAS delivers number of particles within the particle size distribution range, the weighted mean value for particle diameter was used in calculations as $d_{c,wm} = \frac{\sum_{i=1}^m d_i n_i^{av}}{\sum_{i=1}^m n_i^{av}} = 1.014 \pm 0.068 \mu\text{m}$. Here, $m = 6$ is the number of measured diameters of particles; d_i is “ i ”-th measured diameter of particles, μm ; d_i^{av} is the average of 10 values of “ i ”-th measured diameter of particles, μm ; n_i^{av} is the average number of particles with measured diameters d_i ; and 0.068 μm is weighted mean standard deviation. The obtained weighted mean value for particle diameter is in a good agreement with that reported by the manufacturer. According to NIST guidelines,¹⁷ values 4402 and 0.068 μm are adopted as the precision of the PAMAS particle counter for number of particles and diameter, respectively.

IV. SOURCES OF UNCERTAINTIES AND THEIR CONTRIBUTIONS

According to Taylor and Kuyatt,¹⁷ the CSU of the measurement is calculated according to the law of propagation of uncertainty as follows:

$$u_c^2(y) = \sum_{i=1}^N \left(\frac{\partial f}{\partial x_i} \right)^2 u^2(x_i) + 2 \sum_{i=1}^{N-1} \sum_{j=i+1}^N \frac{\partial f}{\partial x_i} \frac{\partial f}{\partial x_j} u(x_i, x_j). \quad (2)$$

When the second term in Eq. (2) is negligible it translates to

$$u_c(y) = \sqrt{\sum_{i=1}^N \left[\left(\frac{\partial f}{\partial x_i} \right) u(x_i) \right]^2}. \quad (3)$$

Since the reduction of filter permeability is caused by the increased amount of attached particles, the uncertainty analysis begins from calculation of uncertainties in parameters from Darcy equation and particle concentrations.

TABLE III. Summary of experimental uncertainty analysis results.

Parameter	Units	CSU	RCSU
A	m^2	6.30×10^{-7}	4.99×10^{-4}
L	m	5.00×10^{-6}	1.24×10^{-3}
R	m	2.50×10^{-6}	1.25×10^{-4}
π	N/A	5.0×10^{-5}	1.59×10^{-5}
V_f	m^3	5.05×10^{-9}	1.74×10^{-3}
$N_{particle}^{PAMAS}$	Particles	4402	1.75×10^{-2}
$d_{c,um}^{PAMAS}$	m	6.84×10^{-8}	6.75×10^{-2}
σ_{at}	m^3	3.56×10^{-9} to 5.98×10^{-8}	7.70×10^{-2}
σ_{cr}	N/A	$(1.40$ to $2.11) \times 10^{-2}$	$(7.75$ to $7.94) \times 10^{-2}$
Δp	Pa	7.80×10^0	2.6×10^{-3}
p	Pa	3.0×10^4	8.8×10^{-3}
p_w	Pa	3.0×10^4	8.8×10^{-3}
Q	m^3/s	1.67×10^{-9}	2.0×10^{-2}
T_A	K	1.0	N/A
T_B	K	2.2×10^{-2}	N/A
T	K	1.0	3.4×10^{-3}
μ_P	$\mu Pa \times s$	5.77×10^{-3}	6.19×10^{-6}
μ_T	$\mu Pa \times s$	21.8	2.34×10^{-2}
μ	$\mu Pa \times s$	21.8	2.34×10^{-2}
k	m^2	2.55×10^{-15}	3.09×10^{-2}
U	m/s	2.64×10^{-6} to 2.64×10^{-5}	2.00×10^{-2}
ϕ	N/A	8.30×10^{-4}	1.92×10^{-3}
ϕ_c	N/A	2.65×10^{-2}	7.39
$\sigma_{cr}^{0, OLSM}$ or a^{OLSM}	N/A	1.57×10^{-2}	5.68×10^{-2}
b^{OLSM}	$(m/s)^{-2}$	1.58×10^5	2.46×10^{-1}
U_{min}^{OLSM}	m/s	9.92×10^{-5}	1.51×10^{-1}
$\sigma_{cr}^{0, WLSM}$ or a^{WLSM}	N/A	1.13×10^{-2}	4.11×10^{-2}
b^{WLSM}	$(m/s)^{-2}$	1.50×10^5	2.38×10^{-1}
U_{min}^{WLSM}	m/s	7.96×10^{-5}	1.39×10^{-1}
σ_{cr}^{model} Eqs. (13) and (15)	N/A	4.32×10^{-3} to 1.16×10^{-2}	4.23×10^{-2} to 1.03×10^{-1}
σ_{cr}^{model} Eqs. (14) and (16)	N/A	1.14×10^{-2}	4.16×10^{-2} to 1.55×10^{-1}

A. Filter length, cross-sectional area, and volume

Glass filter dimensions were measured by a calliper with an uncertainty of $u(L) = 2u(R) = 5 \times 10^{-6}$ m. Using Eq. (3), CSUs for the cross-sectional area and volume of the filter were equal to $u_c(A) = 6.28 \times 10^{-7}$ m and $u_c(V_f) = 5.31 \times 10^{-9}$ m³, respectively.

B. Total volume of attached particles and critical retention concentration

Critical retention concentration, σ_{cr} , is calculated according to the following formula: $\sigma_{cr} = \frac{\sigma_{at}}{V_f}$, where σ_{at} - is the volumetric concentration of attached particles, m³. Cumulative volume of particles attached to the filter is calculated as the sum of incremental volumes of particles attached at various flowrates. Since each consecutive deposited volume of colloids is added to the previous one, $u_c(\sigma_{at})$ is calculated according to the rules of propagation of uncertainties resulting in the CSU of the next cumulative volume of particles being greater than that for the previous one. As calculated, CSUs for σ_{cr} varies from 1.40×10^{-2} (corresponding to 100 ml/min) to 2.11×10^{-2} (corresponding to 10 ml/min), with relative combined standard uncertainty (RCSU), $\delta_c(\sigma_{cr})$, varying from 7.75% to 7.94% (see Table III).

C. Pressure and differential pressure measurements

Pressure of suspension passing through the glass filter without a significant error is determined as

$$p_w = p - \frac{\Delta p}{2}, \quad (4)$$

where p is the pressure measured by PA 33X, and Δp is the differential pressure across the glass filter measured by the respective DPT. Parameters in Eq. (4) correspond to those in Eq. (3) as follows: $y = p_w$, $x_1 = p$ and $x_2 = \Delta p$. Each variable in Eq. (4) contributes to CSU for pressure according to Eq. (3) as follows:

$$\begin{aligned} u_c(p_w) &= \sqrt{\left[\frac{\partial p_w}{\partial p} u(p) \right]^2 + \left[\frac{\partial p_w}{\partial (\Delta p)} u(\Delta p) \right]^2} \\ &= \sqrt{[1 \times u(p)]^2 + \left[-\frac{1}{2} u(\Delta p) \right]^2}. \end{aligned} \quad (5)$$

Using data from Table III, the value of CSU in pressure is calculated as $u_c(p_w) \cong u_c(p) \cong 3.0 \times 10^4$, Pa, since $u_c(p) \gg u_c(\Delta p)$. Thus, determined $u_c(p_w)$ will be used for the

evaluation of uncertainty in density and dynamic viscosity of NaCl solutions.

D. Dynamic viscosity

Dynamic viscosity data for NaCl aqueous solutions were adopted from Kestin *et al.*²² with an accuracy of $\pm 0.5\%$ in the temperature and pressure range of the present study. Equations for dynamic viscosity correlations for NaCl solutions²² include dynamic viscosity data for pure water which were adopted from Cooper and Dooley.²³ Water density data needed for the evaluation of water viscosity were obtained from Wagner *et al.*²⁴

Combined standard uncertainties in temperature and pressure measurements evaluated earlier in Sec. III B (see Table III) were used to calculate the effect of pressure and temperature variation on dynamic viscosity for NaCl solutions at experimental conditions of 2.00 MPa and 298.15 K. Variation of pressure within its CSU resulted in negligible viscosity variation of $5.77 \times 10^{-3} \mu\text{Pa}\times\text{s}$ or $6.19 \times 10^{-4}\%$.

Temperature effect on dynamic viscosity is greater than that from pressure, reaching $21.8 \mu\text{Pa}\times\text{s}$ or 2.34%, which is adopted as uncertainty for dynamic viscosity.

E. Evaluation of uncertainty in core permeability through uncertainty propagation and Monte Carlo simulations

Darcy's equation is used for calculation of filter permeability in the following form:

$$k = k(Q, \mu, L, A, p_1, p_2) = \frac{Q\mu L}{A(p_1 - p_2)}, \quad (6)$$

where, k is permeability of the filter, in D; A is the cross-sectional area of the filter, in m^2 ; p_1 and p_2 are the inlet and outlet pressure of the stream, respectively, in Pa; Q is volumetric flowrate, in m^3/s ; μ is dynamic viscosity of the fluid, in $\text{Pa}\times\text{s}$; L is the length of the filter over which the fluid is experiencing the pressure drop, in m. Each parameter in Eq. (6) contributes to the CSU in permeability,

$$\begin{aligned} u_c(k) &= \sqrt{\left[\frac{\partial k}{\partial Q}u(Q)\right]^2 + \left[\frac{\partial k}{\partial \mu}u(\mu)\right]^2 + \left[\frac{\partial k}{\partial L}u(L)\right]^2 + \left[\frac{\partial k}{\partial A}u(A)\right]^2 + \left[\frac{\partial k}{\partial (\Delta p)}u(\Delta p)\right]^2} \\ &= \sqrt{\left[\frac{\mu L}{A\Delta p}u(Q)\right]^2 + \left[\frac{QL}{A\Delta p}u(\mu)\right]^2 + \left[\frac{Q\mu}{A\Delta p}u(L)\right]^2 + \left[-\frac{Q\mu L}{A^2\Delta p}u(A)\right]^2 + \left[-\frac{Q\mu L}{A(\Delta p)^2}u(\Delta p)\right]^2}, \end{aligned} \quad (7)$$

where, $u(A)$, $u(\Delta p)$, $u(Q)$, $u(\mu)$, and $u(L)$ are earlier calculated CSUs in cross-sectional area of the filter, pressure drop across the core, suspension volumetric flowrate, water dynamic viscosity, and the length of the filter, respectively. Substituting these CSUs into Eq. (7) we obtain the following value of permeability with its CSU equal to $k = (8.844 \pm 0.274) \times 10^{-14} \text{ m}^2$ ($89.61 \pm 2.77 \text{ mD}$) and RCSU of $\delta(k)$ 3.09%.

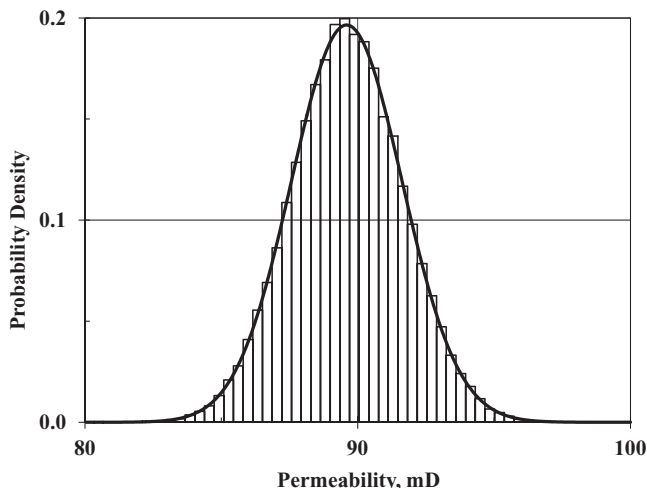


FIG. 4. Monte Carlo simulation results for permeability for an arbitrarily chosen experimental point.

A local sensitivity analysis of Eq. (6), where each parameter was varied one at a time within its CSU, identified two major contributors to CSU in permeability: dynamic viscosity (2.34%) and volumetric flowrate of suspension (2.0%). Reduction of CSU in permeability can be achieved by an increase in the accuracy of temperature measurement and by using a more accurate HPLC pump.

Uncertainty in filter permeability was also evaluated via Monte Carlo simulations using @RISK analysis software (Palisade Corporation, ITHAKA, NY) applied to Eq. (6) with the parameters and their CSUs evaluated earlier (see Table III). Results of this simulations (100 000 iterations) corresponding to the last experimental permeability point from Figure 2 are presented in the form of a histogram in Figure 4 and summarised in Table IV. LogNormal distribution showed the best fit to output results with relative

TABLE IV. Input and output results for Monte Carlo simulations for filter permeability.

Parameter	Monte Carlo simulations results	
	Output results	Log normal distribution results
k_{\min} , mD	81.19	N/A
k_{\max} , mD	98.92	N/A
k_{mean} , mD	89.62	89.61
σ_k , mD	2.72	2.72

standard deviation of $\delta(k) = \frac{\sigma_{LogNorm}(k)}{k_{LogNorm}} \times 100\% = \frac{2.72 \text{ mD}}{89.61 \text{ mD}} \times 100\% \approx 3.04\%$, which excellently agrees with earlier calculated CSU in permeability (3.09%). Time consuming nature of Monte Carlo simulations makes impossible to use this method for real-time permeability variation monitoring.

V. UNCERTAINTIES FOR THEORETICAL MODELS FOR PARTICLE DEPOSITION

A. Evaluation of uncertainty for extrapolated results

A detailed analysis of physical processes governing particle attachment/detachment in porous media at various flowrates was carried out by Bedrikovetsky *et al.*^{25,26} resulting in the mathematical model for the critical retention concentration as a function of velocity,

$$\sigma_{cr}(U) = \sigma_0 \left[1 - \left(\frac{U}{U_{min}} \right)^2 \right], \quad (8)$$

where $\sigma_{cr}(U)$ is the critical retention concentration of colloidal particles; σ_0 is the maximum retention concentration of colloidal particles at zero velocity; U is the velocity, m/s; and U_{min} is the minimum velocity for which no particles can be held on the grain surface by electrostatic and gravity forces, m/s. Equation (8) is used for the determination of σ_0 and U_{min} from the experimental data via extrapolation of the critical retention concentration curve to $U = 0$ and $\sigma_{cr} = 0$.

The model (8) was fitted to the experimental “ σ_{cr} vs U ”-data corresponding to velocities of (3.96, 2.64, and 1.32) $\times 10^{-4}$ m/s. Uncertainty in U was calculated according to Eq. (3) using uncertainties in flowrate and cross-sectional area of the filter. Uncertainty in the critical retention concentration of the attached particles, $u_c(\sigma_{cr})$, was calculated in Sec. IV B. A different approach should be applied for the evaluation of σ_{cr}^0 , $u(\sigma_{cr}^0)$, U_{min} and $u(U_{min})$, since parameters σ_0 and U_{min} cannot be measured directly. Instead, they should be determined by the intersection of the $\sigma_{cr}(U)$ -curve with σ_{cr} -axis via its extrapolation to $U = 0$, and with U -axis via its extrapolation to $\sigma_{cr}^0 = 0$, respectively.

Equation (8) can be re-written as follows:

$$\sigma_{cr}(U) = \sigma_{cr}^0 \left[1 - \left(\frac{U}{U_{min}} \right)^2 \right] = \sigma_{cr}^0 - \frac{\sigma_{cr}^0}{U_{min}^2} U^2 = a - bU^2, \quad (9)$$

and experimental data can be fitted by a quadratic equation using mean-least squares approximation.

Three experimental points are sufficient to fully determine $\sigma_{cr}(U)$ -curve according to Eq. (9). Location of an experimental point along the $\sigma_{cr}(U)$ -curve affects the location of the two intercept points, σ_{cr}^0 and U_{min} , during data extrapolation. Applying an ordinary least squares method (OLSM) to the experimental data and assuming 68.27% confidence interval (which corresponds to \pm one standard deviation) results in the following $\sigma_{cr}^{0,OLSM}$ and U_{min}^{OLSM} values, respectively, 2.765×10^{-1} and 6.565×10^{-4} m/s with their CSUs and RCSUs given in Table III.

During particle attachment experiment one moves to the left along the $\sigma_{cr}(U)$ -curve, then each consecutive $u_c(\sigma_{cr})$ -value incorporates uncertainties from all previous experimental points and movement towards the lower velocities is accompanied by an increase in $u_c(\sigma_{cr})$ -values. Therefore, experimental σ_{cr} -values are of various “quality” which can be quantified by a weighting function $w_i = \frac{1}{[u_c(\sigma_{cr})]^2}$, meaning that the last experimental point on the $\sigma_{cr}(U)$ -curve has the highest uncertainty and the lowest weight. As a result, the above-mentioned three-point curve method gives the lowest possible uncertainty for the last experimental point.

The closer the first experimental point is to U -axis and the last experimental point is to the σ_{cr} -axis, the more accurate U_{min} and σ_0 -values can be determined by extrapolation of the parabolic curve. It is possible to determine the position of the last experimental point before the experiment. However, the location of the first experimental point is problematic since before the experiment it is not possible to predict the minimum velocity at which no particles can be attached to the filter (all particles are swept away by the flowing suspension).

According to Taylor,²⁷ it is appropriate to use the weighted least squares method (WLSM), which gives the most precise estimate of coefficients a and b from Eq. (9). Although some caution has been expressed towards the use of WLSM for non-precisely estimated weights,²⁸ in the present study, uncertainties in the volumes of the attached particles and, consequently, in the critical retention concentrations were accurately calculated within the experimental uncertainty of PAMAS. Applying the WLSM to the quadratic function (9), the following expressions and values for coefficients a , b , and model parameter U_{min}^{WLSM} are obtained with their CSUs and RCSUs listed in Table III:

$$a = \frac{(\sum_{i=1}^n w_i) (\sum_{i=1}^n w_i x_i^2 y_i) - (\sum_{i=1}^n w_i x_i^2) (\sum_{i=1}^n w_i y_i)}{(\sum_{i=1}^n w_i) (\sum_{i=1}^n w_i x_i^4) - (\sum_{i=1}^n w_i x_i^2)^2} = \sigma_{cr}^{0,WLSM} = 2.757 \times 10^{-1} \quad (10)$$

and

$$b = \frac{(\sum_{i=1}^n w_i y_i) (\sum_{i=1}^n w_i x_i^4) - (\sum_{i=1}^n w_i x_i^2 y_i) (\sum_{i=1}^n w_i x_i^2)}{(\sum_{i=1}^n w_i) (\sum_{i=1}^n w_i x_i^4) - (\sum_{i=1}^n w_i x_i^2)^2} = 6.329 \times 10^5 \text{ (m/s)}^{-2}, \quad (11)$$

with $U_{min} = 6.600 \times 10^{-4}$ m/s. The uncertainty in σ_{cr} -values can be calculated via the following expression:

$$u_c^{WLSM}[(\sigma_{cr})_i] = \sqrt{\frac{1}{n-2} \sum_{i=1}^n [(\sigma_{cr})_i - a - bU_i^2]^2} = 3.12 \times 10^{-3}, \quad (12)$$

where $(\sigma_{cr})_i$ is experimental critical retention concentration of colloidal particles.

Although OLSM produced results for σ_{cr} which are in a good agreement with the experimental data, those obtained via WLSM are characterised by relatively smaller errors. Since OLSM treats data without consideration of their uncertainties (or as equally weighed), it underestimates uncertainties in the obtained results. It is, therefore, advisable to use

WLSM for the evaluation of σ_{cr}^0 and U_{min} -values and their uncertainties.

B. Evaluation of uncertainty for particle attachment model

Equation (8) is a simple representation of the two more complex expressions for the critical retention concentration:²⁵

$$\sigma_{cr}^{model}(U) = \left[1 - \left(\frac{h_c}{H} \right)^2 \right] (1 - \phi_c) \phi, \quad (13)$$

$$\sigma_{cr}^{model}(U) = \left[1 - \left(\frac{\mu r_c^2 U}{\phi H F_{ex}} \right)^2 \right] (1 - \phi_c) \phi, \quad (14)$$

where h_c is a cake thickness, which is a function of velocity, m; H is thickness of a rectangular pore channel adopted as $2r_p = 1.3 \times 10^{-5}$ m; F_e - is the total electrostatic force calculated as the sum of attractive London-van der Waals (LvdW) and electric double layer repulsive (DLR), and Born repulsive (BR) forces according to Derjaguin, Landau, Verwey, and Overbeek (DLVO) theory,¹⁹ N; x is the ratio between the drag and electrostatic forces;²⁵ and ϕ_c is porosity of the cake formed on the internal surface of the borosilicate filter due to colloidal particle deposition.

Analysis of model (14) shows that when $U = 0$ m/s, then, $\sigma_{cr}^{model} = (1 - \phi_c)\phi$, meaning that the critical retention concentration depends only on cake and filter porosities. Filter porosity is measured experimentally with the appropriately calculated uncertainty. The maximum value of σ_{cr}^{model} , therefore, greatly depends on adopted the ϕ_c -value. This depends on the assumption of the uniform particle packing (rhombohedral, orthorhombic or cubic, etc.). If the cake porosity is adopted as one of the uniform type of packing, then the appropriate calculations show that, it is not possible to adjust the maximum value of σ_{cr}^{model} to that obtained from extrapolation of the experimental $\sigma_{cr} = \sigma_{cr}(U)$ -curve to the value of $U = 0$ m/s. To overcome such inflexibility of the model (14), the latter was adjusted to the value of $\sigma_{cr}^{max} = \sigma_{cr}^{0, WLSM} = 0.276 \pm 0.006$ (obtained earlier in this paper using WLSM) with ϕ_c as a tuning parameter, resulting in $\phi_c = 0.359 \pm 0.013$. The outcome of this approach is very important: the cake porosity is not adopted via assumptions, but is directly derived from the experimental $\sigma_{cr} = \sigma_{cr}(U)$ -data. Therefore, the uncertainty for the cake porosity is also substantiated by the uncertainty in σ_{cr}^{max} -value derived from experimental critical retention concentrations.

Using Eqs. (3) and (13), CSU in critical retention concentration can be evaluated as follows:

$$\sigma_{cr}^{model}(U) = \sqrt{\left[\left(\frac{2h_c}{H} - \frac{2h_c\phi_c}{H} - \frac{h_c^2}{H^2} + \frac{h_c^2\phi_c}{H^2} \right) u(\phi) \right]^2 + \left[\left(-\frac{2h_c\phi}{H} + \frac{h_c^2\phi}{H^2} \right) u(\phi_c) \right]^2 + \left[\left(\frac{2\phi}{H} - \frac{2\phi\phi_c}{H} - \frac{2h_c\phi}{H^2} + \frac{2h_c\phi\phi_c}{H^2} \right) u(h_c) \right]^2 + \left[\left(-\frac{2h_c\phi}{H^2} + \frac{2h_c\phi\phi_c}{H^2} + \frac{2h_c^2\phi}{H^3} + \frac{2h_c^2\phi\phi_c}{H^3} \right) u(H) \right]^2}. \quad (15)$$

Having evaluated $\sigma_{cr}^{0, WLSM}$ - and U_{min}^{WLSM} -values and their uncertainties, and thus, determined the entire $\sigma_{cr} = \sigma_{cr}(U)$ -curve, it is now possible to determine $\sigma_{cr}^{model} = \sigma_{cr}^{model}(U)$ -curve according to Eqs. (13) and (14). In order to evaluate uncertainties in the values of critical retention concentrations derived from the models (13) and (14), $u(\sigma_{cr}^{model})$, it is necessary to know uncertainties in the parameters of these models.

The only parameter in Eq. (13) which varies with velocity is the cake thickness, h_c . This parameter can be evaluated by fitting Eq. (13) to experimental data, with obtained results in Figure 5 showing a gradual increase in the internal cake thickness accompanied with an increase in critical retention concentration. For the colloidal particle with $d_{c,wm} = 1.014 \pm 0.068 \mu\text{m}$ one-layer cake thickness can be evaluated with the uncertainty of $u_c(h_c^{1layer}) = \pm 0.068 \mu\text{m}$. The number of layers of deposited particles in the cake, n_l , is determined by the ratio between h_c and the mean particle diameter resulting in values varying from 0 to 13, when velocity

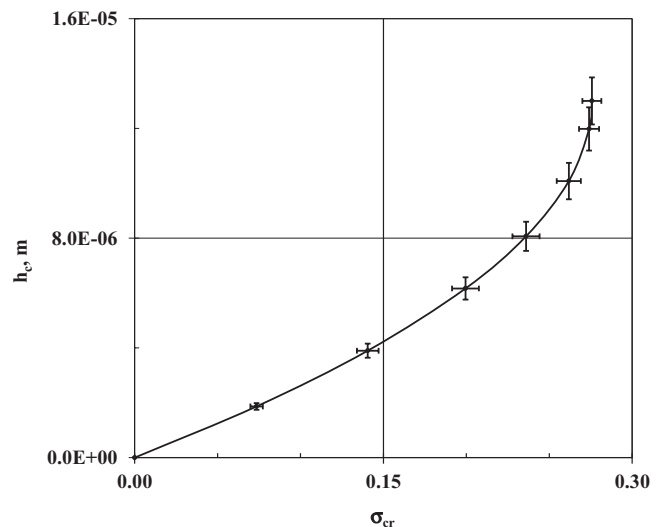


FIG. 5. Variation of cake thickness during particle deposition.

changes from 0 to 6.6×10^{-4} m/s. Uncertainties for the varying cake thickness are calculated according to the following formula $u_c(h_c^m) = \pm 0.068n_l \mu\text{m}$ (see Table III). Uncertainty in particle radius, $u_c(r_c)$, is taken from Table III. Since the glass filter is characterised by a pore width from 10 to 16 μm with $H_{\text{mean}} = 13 \mu\text{m}$, then a standard deviation of 1.0 μm is adopted as $u_c(H)$. Using uncertainties for masses of dry and water-saturated filter, CSU in its porosity is equal to $u_c(\phi) = 8.30 \times 10^{-4}$.

After introducing the values of all parameters and their uncertainties into Eq. (15), we obtained $u(\sigma_{cr}^{\text{model}})$ varying from 4.23 to 10.3% when velocity changes from 0 to 6.6×10^{-4} m/s (see Table III). A local sensitivity analysis was performed to determine how variation of uncertainties in parameters from Eqs. (13) and (14) affects $u(\sigma_{cr}^{\text{model}})$. When we doubled uncertainties for parameters one at a time, $(\sigma_{cr}^{\text{model}})$ remained unchanged for all parameters, but for $u_c(\phi_c)$ it was doubled. Varying parameters in Eqs. (13) and (14) one at a time within their CSUs, we arrive to the conclusion

that ϕ_c has the highest impact on $\sigma_{cr}^{\text{model}}$ according to data presented in Table V. The procedure proposed in the present paper for the evaluation of $u_c(\phi_c)$ via experimental uncertainties in σ_{cr} resulted in the lowest possible $u_c(\phi_c)$ -value for the present experimental conditions, and is, therefore, recommended for calculations.

Using Eqs. (3) and (14) it is possible to evaluate $u(\sigma_{cr}^{\text{model}})$ according to Eq. (16). Additional assumptions should be made before calculating $u(\sigma_{cr}^{\text{model}})$. The resultant electrostatic force is calculated as the derivative of the potential energy. For many parameters of the LvdW, DLR, and BR forces, it is not always possible to calculate their uncertainties. Values of Hamaker constants calculated via DLVO theory often disagree with those obtained experimentally,²⁹ reaching, for example, 50% for non-retarded region of ≤ 10 nm.³⁰ Direct measurements of vdW forces produced results with standard deviation ranging from 14.9% to 23.1%³¹ and uncertainty of 15%.³² In the present study, uncertainty in electrostatic force, $u_c(F_e)$ was adopted as 15%:

$$\sigma_{cr}^{\text{model}}(U) = \sqrt{\left[\left(1 - \phi_c + \frac{1 - \phi\phi_c}{\phi^2} \left(\frac{\mu r_c^2 U}{H F_e x} \right)^2 \right) u(\phi) \right]^2 + \left[\left(-\phi + \frac{1}{\phi} \left(\frac{\mu r_c^2 U}{H F_e x} \right)^2 \right) u(\phi_c) \right]^2 + \left[\left(\frac{2\mu(\phi_c - 1)}{\phi} \left(\frac{r_c^2 U}{H F_e x} \right)^2 \right) u(\mu) \right]^2 + \left[\left(\frac{4r_s^3(\phi_c - 1)}{\phi} \left(\frac{\mu U}{H F_e x} \right)^2 \right) u(r_c) \right]^2 + \left[\left(\frac{2U(\phi_c - 1)}{\phi} \left(\frac{\mu r_c^2 U}{H F_e x} \right)^2 \right) u(U) \right]^2 + \left[\left(\frac{2(1 - \phi_c)}{\phi H^3} \left(\frac{\mu r_c^2 U}{F_e x} \right)^2 \right) u(H) \right]^2 + \left[\left(\frac{2(1 - \phi_c)}{\phi F_e^3} \left(\frac{\mu r_c^2 U}{H x} \right)^2 \right) u(F_e) \right]^2 + \left[\left(\frac{2(1 - \phi_c)}{\phi x^3} \left(\frac{\mu r_c^2 U}{H F_e} \right)^2 \right) u(x) \right]^2 + \left[\left(\frac{2(1 - \phi_c)}{\phi x^3} \left(\frac{\mu r_c^2 U}{H F_e} \right)^2 \right) u(x) \right]^2 \right. \quad (16)$$

According to our calculations, h_c varies from 1.3×10^{-5} to 0 m when fluid velocity changes from 0 to its maximum value of 6.60×10^{-4} m/s, corresponding to the condition

TABLE V. Results of sensitivity analysis for Eqs. (13) and (14).

Parameter	Variation of $\sigma_{cr}^{\text{model}}$, %	
	Equation (13)	Equation (14)
μ	N/A	0.006
r_s	N/A	0.016
U	N/A	0.013
H	0.325	0.019
h_c	0.153	N/A
F_e	N/A	0.038
x	N/A	0.038
ϕ	0.193	0.193
ϕ_c	4.13	4.13

when $\sigma_{cr} = 0$ and all particles are swept away by high-velocity fluid. In this range of “particle-to-surface distances” and for the present experimental conditions, F_e calculated according to DLVO theory²⁵ varies from 2.72×10^{-21} to -9.38×10^{-19} N.

According to Bedrikovetsky *et al.*,²⁵ parameter x is the ratio between the drag and electrostatic forces, with the drag force determined according to the following formula:

$$F_d = \frac{\omega \pi r_c^2 U}{H}, \quad (17)$$

where ω is the dimensionless empirical drag coefficient. The drag coefficient was adopted as 21 via fitting equation (14) to the experimental critical retention concentration data. Applying formula (3) to (17), we obtain that $u_c(F_d)$ varies in the range from 1.26×10^{-15} to 1.66×10^{-14} N and $u_c(x)$

from 2.73×10^6 to 1.12×10^5 for the above range of fluid velocities.

After substitution of all relevant parameters into Eq. (16) we obtained that RCSU (σ_{cr}^{model}) varies from 4.16% to 15.5% for the same range of fluid velocities (see Table III). Model (14) represents experimental $\sigma_{cr} = \sigma_{cr}(U)$ -data less accurately than model (13) due to the presence in Eq. (14) of the attractive electrostatic force, whose value and uncertainty cannot be reliably established due to unavailability of dielectric data.

VI. CONCLUSIONS

Calculation of experimental uncertainties for permeability of a borosilicate filter was carried out through propagation of uncertainties for parameters in Darcy's equation and also, using Monte-Carlo simulations. Both methods provided identical values for combined standard uncertainty for permeability. The local sensitivity analysis of Darcy equation showed that the uncertainties in dynamic viscosity and volumetric flowrate of colloidal suspension have the highest impact on the overall uncertainty for filter permeability.

The uncertainty in each consecutive value of critical retention concentration incorporates uncertainties from all previous values. Therefore, the total number of experimental points for critical retention concentrations, as a function of velocity, should be limited to three points in order to reduce the uncertainty in the determination of maximum critical retention concentration. Weighing functions for the critical retention concentrations were accurately calculated through the propagation of uncertainties in the respective experimental parameters. Application of the weighted least squares method resulted in more accurate values for maximum critical retention concentration and minimum velocity.

The local sensitivity analysis of the models showed that internal cake porosity has a significant impact on the modelling results and their uncertainties. The first model, containing the internal cake thickness as one of its parameters, represented experimental critical retention concentration data better than the second model which used dynamic viscosity, particle radius, pore thickness, drag, and total electrostatic forces as model parameters. Higher deviations of the results from the second model are, probably, due to the presence of the total electrostatic force in the model's formula. The values and uncertainty for this force cannot be reliably measured and calculated, due to lack of experimental dielectric data at the current experimental conditions.

The proposed uncertainty analysis was implemented into Microsoft Excel™ spreadsheet coupled with the real-time data acquisition software, such that each experimental data point is accompanied by its uncertainty, leading to timely decisions during particle attachment experiments.

Overall, the presented method for the evaluation of experimental and modelling uncertainties establishes the validity ranges for experimental permeability and particle attachment data and for the corresponding theoretical models. This makes possible intra- and inter-laboratory data comparison which is the first step towards standardizing these types of experiments.

ACKNOWLEDGMENTS

Authors thank Institute of Minerals and Energy Resources (IMER) of the University of Adelaide for financial support. Financial support from the Australian Research Council (ARC) Discovery Project 1094299, ARC Linkage Project 100100613, and Santos Pty. Ltd. is gratefully acknowledged.

- ¹C. Gruesbeck and R. E. Collins, *Soc. Pet. Eng. J.* **22**, 847–856 (1982).
- ²N. Tufenkji and M. Elimelech, *Langmuir* **20**(25), 10818–10828 (2004).
- ³A. Santos and P. Bedrikovetsky, *Comput. Appl. Math.* **23**(2–3), 259–284 (2004).
- ⁴O. Kwon, A. K. Kronenberg, A. F. Gangi, and B. Johnson, *J. Geophys. Res.* **106**(B9), 19339–19353, doi:10.1029/2001JB000273 (2001).
- ⁵O. Kwon, B. E. Herbert, and A. K. Kronenberg, *J. Geophys. Res.* **109**, B10205, doi:10.1029/2004JB003052 (2004).
- ⁶O. Kwon, B. E. Herbert, and A. K. Kronenberg, *J. Geophys. Res.* **109**, B10206, doi:10.1029/2004JB003055 (2004).
- ⁷C. Dong, *J. Manuf. Sci. Eng.* **127**(4), 907–911 (2005).
- ⁸S. Mazumder and K. H. Wolf, *Int. J. Coal Geol.* **74**(2), 123–138 (2008).
- ⁹A. S. El-Dieb and R. D. Hooton, *Cem. Concr. Res.* **24**(5), 854–862 (1994).
- ¹⁰G. Brighenti and P. Macini, *Future Groundwater Resources at Risk* (IAHS, Helsinki, Finland, 1994), Vol. 222, pp. 409–416.
- ¹¹American Petroleum Institute, *Recommended Practices for Core Analysis: Recommended Practice*, 2nd ed. (American Petroleum Institute Publishing Service, 1998), Vol. 40.
- ¹²A. C. Payatakes, R. Rajagopalan, and C. Tien, *Can. J. Chem. Eng.* **52**(6), 722–731 (1974).
- ¹³A. Santos and P. Bedrikovetsky, *TPM* **62**(1), 23–53 (2006).
- ¹⁴A. A. Shapiro, P. G. Bedrikovetsky, A. Santos, and O. O. Medvedev, *TPM* **67**(1), 135–164 (2007).
- ¹⁵P. Bedrikovetsky, *TPM* **75**, 335–369 (2008).
- ¹⁶F. A. H. Al-Abduwani, R. Farajzadeh, W. M. G. T. van den Broek, P. K. Currie, and P. L. J. Zitha, *Rev. Sci. Instrum.* **76**, 103704 (2005).
- ¹⁷B. N. Taylor and C. E. Kuyatt, "Guidelines for evaluating and expressing the uncertainty of NIST measurement results," National Institute of Standards and Technology Technical Note 1297 (U.S. Government Printing Office, Washington, DC, 1994).
- ¹⁸"Quantifying uncertainties in analytical measurements," *EURACHEM/CITAC Guide CG4*, edited by S. L. R. Ellison, M. Rosslein, and M. Williams (EURACHEM, 2000).
- ¹⁹B. Derjaguin and L. Landau, *PrSS* **43**(1–4), 30–59 (1993).
- ²⁰J. Bergendahl and D. Grasso, *AIChE J.* **45**(3), 475–484 (1999).
- ²¹D. Ripple, G. W. Burns, and M. G. Scroger, "Assessment of uncertainties of thermocouple calibrations at NIST," NISTIR 5340 (National Institute of Standards and Technology, Gaithersburg, MD, 1994), p. 35.
- ²²J. Kestin, H. E. Khalifa and R. J. Correia, *JPCRD* **10**(1), 71–87 (1981).
- ²³J. R. Cooper and R. B. Dooley, *The International Association for the Properties of Water and Steam* (Berlin, Germany, 2008), p. 9.
- ²⁴W. Wagner, J. R. Cooper, A. Dittmann, J. Kijima, H.-J. Kretzschmar, A. Kruse, R. Mares, K. Oguchi, H. Sato, I. Stocker, O. Sifner, Y. Takaiishi, I. Tanishita, J. Trubenbach, and T. Willkommen, *J. Eng. Gas Turbines Power* **122**, 150–182 (2000).
- ²⁵P. Bedrikovetsky, F. D. Siqueira, C. Furtado, and A. L. S. de Souza, *TPM* **86**(2), 353–383 (2011).
- ²⁶P. Bedrikovetsky, A. Zeinjahromi, F. D. Siqueira, C. A. Furtado, and A. L. S. de Souza, *TPM* **91**, 173–197 (2012).
- ²⁷J. R. Taylor, *An Introduction to Error Analysis: The Study of Uncertainties in Physical Measurements* (University Science Books, New York, 1982).
- ²⁸R. J. Carroll and D. Ruppert, *Transformation and Weighing in Regression* (Chapman and Hall, New York, 1988).
- ²⁹Q. Qi and G. J. Brereton, *ITUFF* **42**(4), 619–629 (1995).
- ³⁰D. Chan and P. Richmond, *Proc. R. Soc. London, Ser. A* **353**(1673), 163–176 (1977).
- ³¹J. A. Kitchener and A. P. Prosser, *Proc. R. Soc. London, Ser. A* **242**(1230), 403–409 (1957).
- ³²A. K. Mohapatra and C. S. Unnikrishnan, *EL* **73**(6), 839–845 (2006).